Journal of Power Sources 195 (2010) 4634–4640

Contents lists available at ScienceDirect

Journal of Power Sources

journal homepage: www.elsevier.com/locate/jpowsour

A facile and novel approach toward synthetic polypyrrole oligomers functionalization of multi-walled carbon nanotubes as PtRu catalyst support for methanol electro-oxidation

Yanchun Zhao*, Xiulin Yang, Jianniao Tian, Fengyang Wang, Lu Zhan

Key Laboratory for the Chemistry and Molecular Engineering of Medicinal Resources (Ministry of Education of China), College of Chemistry and Chemical Engineering, Guangxi Normal University, Yucai Road, No. 15, Guilin 541004, Guangxi, PR China

ARTICLE INFO

Article history:
Received 2 January 2010
Accepted 10 February 2010
Available online 16 February 2010

Keywords:
PtRu nanoparticles
Multi-walled carbon nanotubes
Polypyrrole oligomers
Electrocatalysis
Fuel cells

ABSTRACT

A new process to prepare well-dispersed PtRu nanoparticles on polypyrrole oligomers (PPO)-functionalized multi-walled carbon nanotubes (PtRu/PPO-MWCNTs) is reported. In this method, bimetallic PtRu electrocatalysts are deposited onto polypyrrole oligomers (PPO)-functionalized MWCNTs by polyol process. The noncovalent functionalization of MWCNTs by PPO is simple and can be carried out at room temperature without the use of expensive chemicals or corrosive acids, thus preserving the integrity and the electronic structure of MWCNTs. PtRu electrocatalysts on PPO-functionalized MWCNTs show much better distribution with no formation of aggregates, higher electrochemically active surface area, and higher electrocatalytic activity and stability for the electro-oxidation of methanol in direct methanol fuel cells as compared to those on conventional acid-treated MWCNTs and carbon black supported PtRu electrocatalysts. It is implied in the study that the method of PPO-functionalized MWCNTs with Pt-based catalysts is promising and will be potential in design and fabrication of electrocatalysis.

1. Introduction

Carbon nanotubes (CNTs) including single wall carbon nanotubes (SWCNTs) and multi-walled carbon nanotubes (MWCNTs) have captured the attention of researchers worldwide due to their unique properties, such as high external surfaces, good electronic conductivity, large surface to volume ratio and high stability, which make CNTs an ideal supporting material [1,2]. In recent years, considerable efforts have been devoted to anchor noble metal particles (such as Pt, PtRu, etc.) onto the framework of CNTs for their application in the area of catalysis [3,4]. However, the deposition, distribution, and size of Pt-based nanoparticles supported on CNTs depend strongly on the surface treatment and surface properties of CNTs. The activity of Pt-based nanoparticles is also significantly affected by the nature of their interaction with CNTs and the intrinsic properties of CNTs. Since pristine CNTs are chemically inert, it is necessary to activate the graphitic surface of the nanotubes in order to anchor and deposit catalytic nanoparticles. CNTs are usually functionalized by harsh oxidative processes, such as refluxing in the mixture of HNO_3 and H_2SO_4 to generate defects on the sidewalls and tube tips, those defects can serve as anchor groups for functionalization and/or can provide sites for the coordination chemistry [5,6]. However, due to the introduction of a large number of defects, such chemical oxidation method reduces the electrical conductivity and corrosion resistance of CNTs. Corrosion of carbon or CNT supports has been identified as one of the main reasons for the loss of the electrochemical active surface area of Pt-based electrocatalysts and the reduced durability during fuel cell operation [7]. Therefore, development of a better and more effective functionalization method that can not only introduce high density and homogeneous surface functional groups but also has little or no structural damage to CNTs remains a major challenge.

Recently, noncovalent functionalization of CNTs has attracted particular attention because it enables the properties of the hybrids of nanoparticles and CNTs to be tailored while still preserving nearly all the intrinsic properties of CNTs. Guided by the structures of the functional molecules on the CNTs, we will summarize the recent work carried out by ourselves and others under the umbrella of the following three subtopics: (i) aromatic small-molecule-based noncovalent functionalization [8–10], (ii) bio-macromolecule-based noncovalent functionalization [11–13], and (iii) polymer-based noncovalent functionalization [14,15]. In these approaches, noncovalent modifications of CNTs can do much to preserve their desired properties, while improving their solubility quite remarkably.

Moreover, due to the existence of various oxidation structures, electrically conducting polymers, such as polyaniline (PANi), polypyrrole (PPy), polythiophene (PTh) and their derivatives have

* Corresponding author. Tel.: +86 773 5846279; fax: +86 773 5832294.
E-mail address: yanchunzh@yahoo.cn (Y. Zhao).

0378-7753/$ – see front matter © 2010 Elsevier B.V. All rights reserved.
doi:10.1016/j.jpowsour.2010.02.023

been considered as promising materials for supercapacitors [16], electrochemical sensor [17], modification agent [18] and so on. Among them, conducting polypyrrole (PPy) has been the focus of a great deal of research for catalytic materials application in recent years because its superior properties that include high electric conductivity, high specific capacitance (easy up to 100 F g^{-1}) and good chemical and thermal stability, especially facile synthesis and environmentally friendly. It can be prepared by two main routes, i.e. the chemical [18–22] and electrochemical oxidation [23–25] of pyrrole in various organic solvents and in aqueous media. Regarding the chemical oxidative polymerization of the pyrrole monomer, many oxidants have been used: such as ferric chloride, hydrogen peroxide, and ammonium peroxydisulfate. Most of these reports need to be conducted in lower temperature and will introduce lots of impurity ions from the oxidants. However, the preparation of MWCNTs modified by polypyrrole oligomers without addition any oxidants at room temperature is rarely reported, especially as supports applied for direct methanol fuel cells. So this research work will be of great significance.

In this study, we report a simple chemical polymerization of pyrrole monomer on MWCNTs with coverage of PtRu nanoparticles. By this method, well-dispersed PtRu nanoparticles can be directly loaded onto the MWCNT walls. It was found that PtRu nanoparticles on PPO-functionalized MWCNTs have higher electrochemical surface area and better activity for methanol electrochemical oxidation in acid solution than that supported on acid-oxidized MWCNTs and carbon black. In addition, significantly enhanced stability for the methanol electro-oxidation was also observed for the PtRu nanoparticles supported on PPO-functionalized MWCNTs.

2. Experimental

2.1. Materials

All chemical reagents used in this experiment were of analytical grade. Sulfuric acid, nitric acid, ethanol, methanol, $H_2PtCl_6{\cdot}6H_2O$, $RuCl_3$, ethylene glycol and pyrrole were procured commercially and were used as received without further purification. The raw-MWCNTs were purchased from Shenzhen Nanotechnologies Port Co. Ltd. (Shenzhen, China) with the diameters of 40–60 nm, lengths of 5–15 μm, and purity of 98%. Vulcan XC-72 carbon black was purchased from Cabot Corporation.

2.2. PPO- and acid-functionalization of MWCNTs

The procedure for the noncovalent functionalization of MWCNTs using PPO is as follows: first, 100 mg of pristine MWCNTs was sonicated in 40 mL of ethanol–water (1:1, v/v ratio) containing 1.0 mL pyrrole and 1.0 mL 1.0 M HCl at room temperature for 30 min and then the obtained solution was under vigorous stirring for three days. The above solution was centrifuged and washed with ethanol and water 3 times, respectively. The as-functionalized MWCNTs were dried in a vacuum oven at 70 °C for 12 h and then the PPO-MWCNTs were obtained. As a comparison, MWCNTs were also functionalized by a conventional acid treatment. In this treatment, the MWCNTs were first dispersed in a concentrated H_2SO_4–HNO_3 mixture (8.0 M for each acid) and then placed in an ultrasonic bath for treatment at a bath temperature of 60 °C with duration of 2 h. The acid-treated MWCNTs were washed for several times and dried in a vacuum oven at 70 °C for 12 h and collected (denoted as AO-MWCNTs).

2.3. Synthesis of PtRu/MWCNTs electrocatalysts

To deposit the PtRu nanoparticles on the walls of the PPO-functionalized MWCNTs (20 wt.% metal content, atomic ratio of Pt:Ru = 1:1), the PPO-functionalized MWCNTs were placed in a 50 mL flask, to which 30.0 mL of ethylene glycol–water solution (2:1, v/v ratio) was added. An appropriate amount of stock solutions (10 mM) of the precursors was added, depending on the expected weight loadings and compositional ratios of each metal. The reduction reactions were performed under reflux conditions for 2 h with continuous magnetic stirring. The catalysts were then separated from the solution in a centrifuge and thoroughly washed with deionized water. The obtained PtRu nanoparticles on PPO-functionalized MWCNTs (PtRu/PPO-MWCNTs) were dried in a vacuum oven at 70 °C for 12 h. PtRu nanoparticles on acid-functionalized MWCNTs (PtRu/AO-MWCNTs) and carbon black (PtRu/C) were prepared using similar procedures as described above.

2.4. Characterization

FT-IR (Perkin-Elmer, America) and UV–vis absorption spectra (TU-1901, China) were employed to analyze the surface chemical compositions of the purified PPO-MWCNTs composite. The Raman spectrum (invia, Renishaw, England) was also used to study the integrity and electronic structure of the samples. Morphology and microstructure of the synthesized materials was investigated by TEM (FEI TECNAI G^2 12, Holand). XRD analysis data from the samples were collected using a Rigaku D/MAX 2500 v/pc (Japan) diffractometer with Cu Kα radiation. Electrochemical measurements were recorded using CHI 660C electrochemical working station (CH Instrument, Inc.), and a conventional three-electrode system was used throughout this work.

2.5. Electrochemical measurement

The electrochemical activity of PtRu/PPO-MWCNTs, PtRu/AO-MWCNTs, and PtRu/C electrocatalyst was measured for the electro-oxidation of methanol. As a typical process, 2.0 mg of electrocatalyst sample was ultrasonically mixed in 400 μL of ethanol–water solution (1:1, v/v ratio) to form a homogeneous ink followed by dropping 5 μL of the electrocatalyst ink onto the surface of a glassy carbon electrode (GCE, with a diameter of 3 mm). Then, 5 μL of Nafion solution of 0.5% in ethanol was added to fix the electrocatalyst on the GCE surface. Pt sheet and a saturated calomel electrode (SCE) were used as the counter and reference electrodes, respectively. All potentials in the present study were given versus SCE reference electrode. The electrochemical surface area (EAS) was assessed using CO-stripping techniques in 0.5 M H_2SO_4 solution. Initially, nitrogen was purged to the 0.5 M H_2SO_4 solution for 15 min. Afterwards, the adsorption of CO was performed by purging high-purity CO (99.9% purity) gas to the solution for 10 min while maintaining the potential at −0.16 V. Then, the dissolved CO in the solution was removed by bubbling nitrogen gas into the solution for 20 min by holding the potential at −0.16 V. Finally, the stripping voltammograms were collected between −0.2 and 1.0 V with a scan rate of 50 mV s^{-1}. The elelctrocatalytic activity for the methanol oxidation reaction was measured in a nitrogen–saturated 0.5 M H_2SO_4 + 1.0 M CH_3OH solution at a scan rate of 50 mV s^{-1}. Several activation scans were performed until reproducible voltammograms were obtained, and only the last cycles were used for comparison of the catalytic activity. The Pt metal loading was kept at 3.26 μg and all tests were conducted at ambient temperature (26 ± 1 °C).

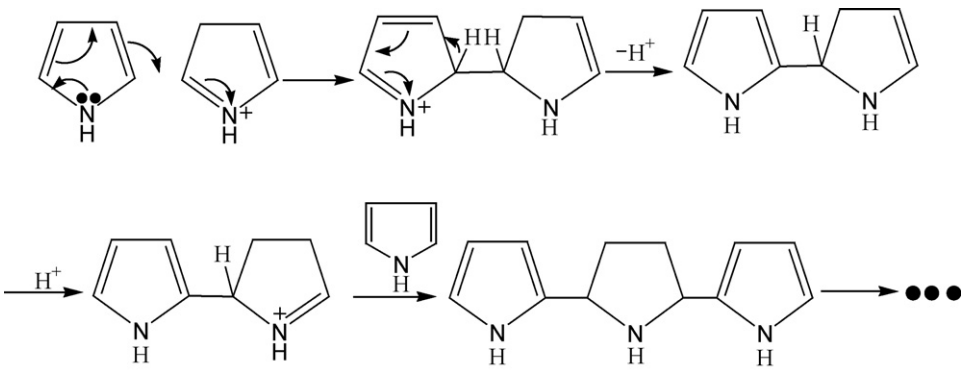

Scheme 1. Mechanism of chemical polymerization of pyrrole.

3. Results and discussion

3.1. The mechanism about formation of polypyrrole oligomers (PPO)

Fine polypyrrole oligomers (PPO) were fabricated by a single-step polymerization of pyrrole monomer when appropriate hydrochloric acid was added into the reaction solution under vigorous stirring for three days [26]. The first step of the reaction is the protonation of pyrrole to form a radical cation, which then reacts with another monomer molecule to form a dimer [27]. The single charged dimer can then lose one protons to rearomatize and form a stable dimer, which is more easily protonation than the monomer and may participate in additional radical coupling reactions to form oligomers and eventually polymer. The synthesis of the polymerization of pyrrole is illustrated in Scheme 1.

3.2. FT-IR, UV–vis and Raman spectra analysis of PPO-functionalized MWCNTs

Fig. 1 displays the FT-IR spectra of raw-MWCNTs (a), PPO (b), and PPO-MWCNTs (c). The spectrum for unmodified MWCNTs (a) shows a weak peak at 3412 cm^{-1} assigned to O–H stretching vibration, which may result from the oxidation of some MWCNTs defects by oxygen in air. FT-IR spectrum for PPO (b) which was prepared according to PPO-MWCNTs without addition MWCNTs shows a typical profile with two peaks at 3389 and 3278 cm^{-1} due to the asymmetrical and symmetrical N–H stretching vibrations [28], the peak at 2923 cm^{-1} due to the stretching of C–H, and the band at 2357 cm^{-1} are attributed to the stretching of C=N [29,30]. The N–H bending in amine is observed at 1634 cm^{-1}, it seems too broad, hence, includes the contributions from C=N imines stretch and possibly C=C alkenes stretching [31]. The two peaks at 1386 and 1316 cm^{-1} are characteristic of the in-plane vibration of pyrrole ring, which indicates the ring structure was not affected by polymerization [24,32]. The peak observed at 1100 cm^{-1} corresponds to the in-plane deformation vibration of NH^+, which is formed on the PPO chains by protonation [33,34]. The strong peak between 700 and 800 cm^{-1}, characteristic of a five-membered aromatic ring, indicates the polymerization degree was low in acid solution without addition another oxidant. Similar results have been reported in ever before [32]. The spectrum of PPO-functionalized MWCNTs dispersion (c) is very similar to that of the PPO alone. In general, aromatic structures are known to interact strongly with the basal plane of the graphitic surface via π-stacking [10,35]. Thus, the π-bonded surface of the MWCNTs might interact strongly with the conjugated structure of PPO, especially through the pyrrole ring. These results confirm that the PPO has been successfully wrapped on the surface of MWCNTs.

To further investigate the PPO-functionalized on the surface of MWCNTs, the UV–vis spectra were obtained. Fig. 2 is the electronic absorption spectra curves of PPO-MWCNTs (a), PPO (b), raw-MWCNTs (c) and pyrrole (d). In this figure, no characteristic absorption peak was observed for the raw-MWCNTs in the range of 200–600 nm [9,36], whereas PPO exhibits bands near 222 and 358 nm. The absorption peak at 222 nm is due to the π–π interactions of benzenoid transitions of the pyrrole ring of PPO,

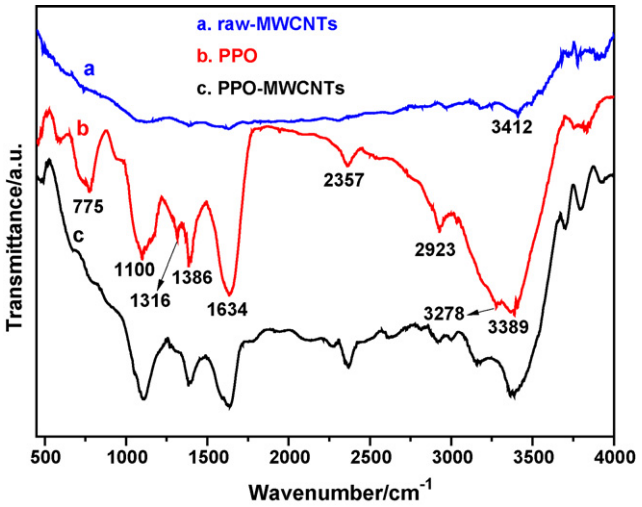

Fig. 1. FT-IR spectra of raw-MWCNTs (a), PPO (b), and PPO-MWCNTs (c).

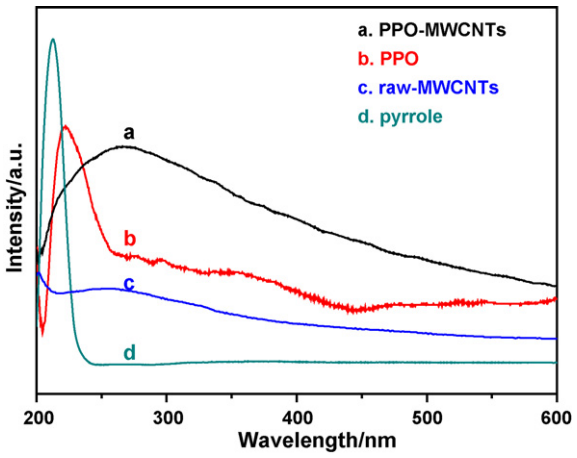

Fig. 2. UV–vis absorption spectra of PPO-MWCNTs (a), PPO (b), raw-MWCNTs (c), and pyrrole (d).

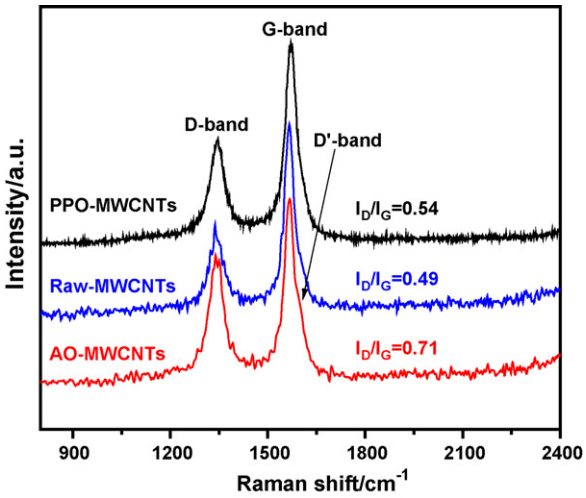

Fig. 3. Raman spectra of PPO-MWCNTs (a), raw-MWCNTs (b), and AO-MWCNTs (c).

while the peak at 358 nm elucidates that the polymerization degree was not very high [32]. Compared to the absorption peak of pyrrole (212 nm), a blue shift was detected, which further illustrated that PPO was formed [37]. Interestingly, the absorption spectra of the PPO-MWCNTs dispersed in ethanol solution show a significantly peak at around ca. 266 nm. Another blue shift was detected compared to the PPO, which was presumably caused by the π–π interactions between the pyrrole ring of PPO and the carbon nanotube sidewalls.

Raman spectroscopy is a powerful tool to characterize the extent of disorder or the degree of crystallinity in the functionalized MWCNTs [38,39]. As shown in Fig. 3, the D- and G-bands at ~1340 and ~1570 cm^{-1}, respectively, attributed to the structure of sp^3 and sp^2 hybridized carbon atom [40], indicating the defects/disorder-induced modes and in-plane vibrations of the graphitic wall, can be clearly observed for raw-MWCNTs, polypyrrole oligomers-functionalized MWCNTs and acid-treated MWCNTs, respectively. Therefore, the degree of the graphitization of MWCNTs can be quantified by the intensity ratio of the D- to G-bands. The peak intensity ratios (I_D/I_G) are 0.54, 0.49 and 0.71 for the PPO-MWCNTs, raw-MWCNTs, and AO-MWCNTs samples, respectively. The D′-band at ~1600 cm^{-1} is barely discernible in raw-MWCNTs and PPO-MWCNTs, while the peaks are more clearly evident in the AO-MWCNTs. It is well-known that the D′-band is also associated with the defects and disorder in carbon nanotubes [41,42]. Thus, the largest I_D/I_G ratio and the enhancement of the D′-band of the AO-MWCNTs sample imply that AO-MWCNTs contain more amorphous carbon impurities than the other two MWCNTs samples [43]. This result implies that the harsh chemical acid treatment produces carboxylic acid sites on the surface, causing significant structural damage of MWCNTs. This would decrease the electrical conductivity of MWCNTs and lower the corrosion resistance, which is consistent with literature [44,45]. In contrast, the PPO functionalization method can preferably preserve the integrity and electronic structure of carbon nanotubes and provides highly effective functional groups on the surface of MWCNTs for the subsequent deposition PtRu nanoparticles.

It is worthy to be noted that the Raman signals of PPO were not detected for the functionalized MWCNTs. Baskaran et al. [46] reported that functionalized MWCNTs prepared by ATRP with a PS content of 33 wt.% also did not exhibit characteristic Raman signals of PS. The absence of PPO signals in our case is possibly due to the low PPO mass densities. After functionalization with PPO, the D- and G-bands show slightly shifts upfield for ~7–9 cm^{-1}, as

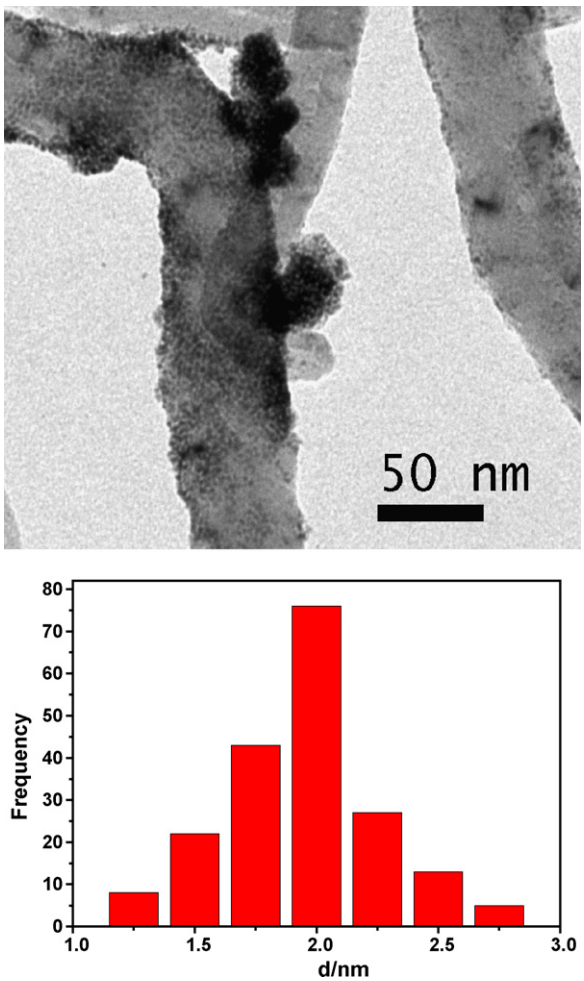

Fig. 4. TEM images and histogram of particle size distribution of the as-obtained PtRu/PPO-MWCNTs catalysts.

compared to that of the raw-MWCNTs and AO-MWCNTs. This shift should be associated with PPO chains noncovalently attached to the MWCNTs surface [47].

3.3. TEM and XRD analysis of PtRu/PPO-MWCNTs

Fig. 4 shows TEM images and the histograms of metal particle size for PtRu/PPO-MWCNTs catalyst. As can be seen, the PtRu alloy nanoparticles with a narrow particle size distribution are well dispersed on the surface of the support. In the study, the mean size of the metal nanoparticles on PPO-MWCNTs support is obtained by measuring 200 randomly chosen particles in the magnified TEM images. For the PtRu alloy catalyst, the mean particle size has a diameter of about 2.0 nm. The values are in good agreement with the XRD data. Despite the small size of the PtRu particles, no nanoparticles aggregation is clearly observed on the nanotube surface, probably because of the large number of nucleation centers available on the surface of the PPO-functionalized MWCNTs. This unique structure appears to provide a suitable support for many uniform PtRu particles, thereby favoring the high performance of methanol oxidation, as discussed below. In addition, energy dispersive spectroscopy (EDS) analysis was utilized to determine the chemical composition of the PtRu/PPO-MWCNTs catalyst. The peaks of Pt, Ru, C and O were observed in Fig. 5 which were the composition of the catalyst. The atom ratio is 2.3% and 2.7% for Ru and Pt, which was consistent with the initial atom ratio of Ru to Pt at 1:1. This indicates that the precursor, $RuCl_3$ and

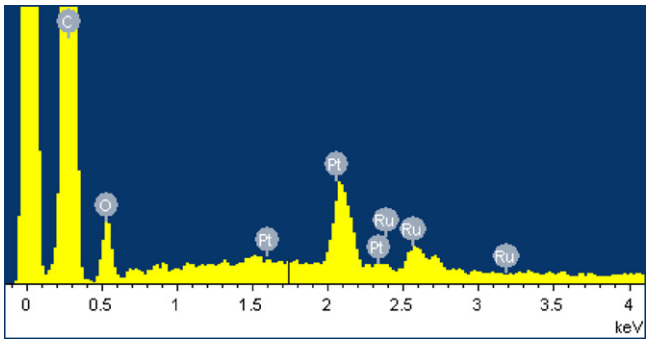

Fig. 5. EDS spectrum of the PtRu/PPO-MWCNTs composites.

$H_2PtCl_6{\cdot}6H_2O$, almost converted completely under the experimental conditions.

The prepared PtRu/PPO-MWCNTs were also characterized by powder X-ray diffraction (XRD), together with the patterns of the PtRu/AO-MWCNTs and PtRu/C composites, as shown in Fig. 6. XRD is a bulk analysis that reveals the crystal structure, lattice constant, and crystal orientation of supported catalysts. The broad peaks at $2\theta = 26.3^\circ$ and 53.9° are associated with the (0 0 2) and (0 0 4) planes of the graphite-like structure of the multi-walled carbon nanotubes [4,14], and the diffraction peaks at $2\theta = 40.0^\circ$, 47.6°, 67.6°, and 81.7° with the d values of 2.2499, 1.9106, 1.3854, and 1.1779 can be attributed to the (1 1 1), (2 0 0), (2 2 0), and (3 1 1) crystalline planes of the face-centered cubic (fcc) structure of the Pt. Diffraction peaks near 38° and 44° in 2θ from Ru are not observed, possibly because Ru has entered the Pt lattice and formed the Pt–Ru alloy or Ru exists as the amorphous form [48,49]. In addition, the broadened diffraction peaks of the metals are strong indication of nanocrystals [50], and the average PtRu particle size is estimated by using the Scherer equation [51,52]. The equation can be expressed as follows:

$$d_{XRD} = \frac{0.9\lambda}{\beta \cos\theta} \quad (1)$$

where d_{XRD} is the average particle size (nm), λ is the wavelength of X-ray (0.15406 nm), θ is the angle at the peak maximum, and β is the width (rad) of the peak at half height. The calculated mean sizes according to the diffraction peak of Pt (1 1 1) are found to be in the range of 2.1, 2.7 and 3.2 nm for PtRu/PPO-MWCNTs, PtRu/AO-MWCNTs and PtRu/C, respectively.

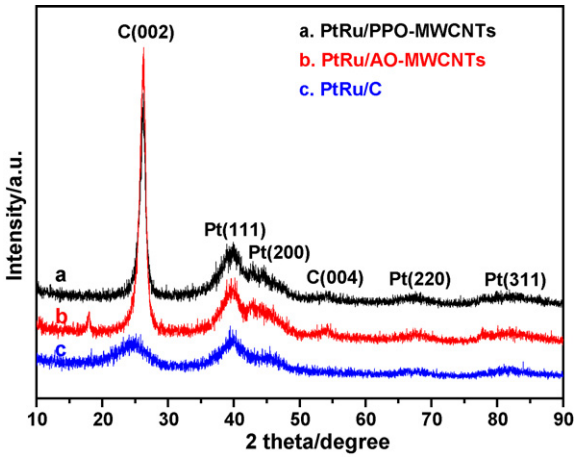

Fig. 6. X-ray diffraction patterns of the PtRu/PPO-MWCNTs (a), PtRu/AO-MWCNTs (b), and PtRu/C (c).

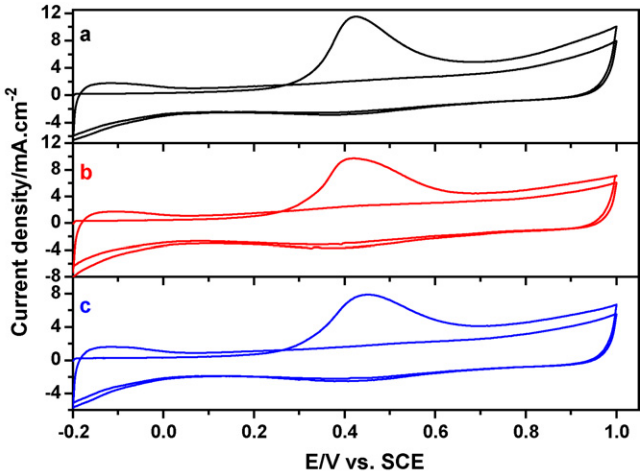

Fig. 7. CO-stripping voltammograms of (a) PtRu/PPO-MWCNTs, (b) PtRu/AO-MWCNTs, and (c) PtRu/C catalysts in 0.5 M H_2SO_4 at room temperature and 50 mV s^{-1} scan rate.

3.4. The electrochemical surface area of the catalysts

CO-stripping voltammetry was performed to compare the electrochemical surface area (ESA) of all the catalysts. Fig. 7 shows the CO-stripping voltammograms and the subsequent cyclic voltammograms (CV) for the PtRu/PPO-MWCNTs (Fig. 7a) and PtRu/AO-MWCNTs (Fig. 7b) along with PtRu on Vulcan XC-72 carbon black (Fig. 7c) catalysts in 0.5 M H_2SO_4 at a scan rate of 50 mV s^{-1}. The adsorption time of CO was set to 10 min, since a further increase in the adsorption time did not change the voltammograms. It can be observed from the voltammogram that for all the catalysts in the first scan the hydrogen desorption peaks are largely suppressed in the lower potential region due to the saturation of the PtRu alloy surface with CO_{ads} species. The CV curves showed a single oxidation peak, whereas no CO oxidation was monitored in the second scan confirming the complete removal of the CO_{ads} species. It has been found that CO adsorbs on Pt through a linear one to one bonding. With Ru in presence, the situation becomes somewhat ambiguous. CO can adsorb on both Pt and Ru sites in the PtRu catalysts. However, most researchers still assume a one to one bonding for Ru sites in PtRu alloys [53]. A charge to metal area conversion factor of 420 μC cm^{-2} for Pt and Ru was therefore adopted to compute the electrochemical active surface areas of the catalysts [54].

$$\text{EAS} = \frac{Q_{CO}}{420\ (\mu\text{C cm}^{-2})} \quad (2)$$

where Q_{CO} is the charge for CO desorption electro-oxidation in microcoulomb (μC), The ESA for the PtRu/PPO-MWCNTs is apparently higher than PtRu/AO-MWCNTs and PtRu/C, most likely due to the smaller size and much better dispersion of the PtRu nanoparticles on PPO-functionalized MWCNTs (in Table 1). This also demonstrates that the PtRu nanoparticles deposited on PPO-MWCNTs are electrochemically more accessible, which is very important for electrocatalyst applications in fuel cells.

Table 1
Electrochemical surface area, onset potential, forward peak current and peak ratio of different PtRu electrocatalysts on PPO-MWCNTs, AO-MWCNTs and carbon black.

Electrocatalyst	ESA ($m^2\ g^{-1}$)	Onset potential (V)	Forward peak current (mA cm^{-2})	I_f/I_b
PtRu/C	27.8	0.33	10.5	1.06
PtRu/AO-MWCNTs	30.9	0.26	16.2	1.18
PtRu/PPO-MWCNTs	38.1	0.19	27.8	1.24

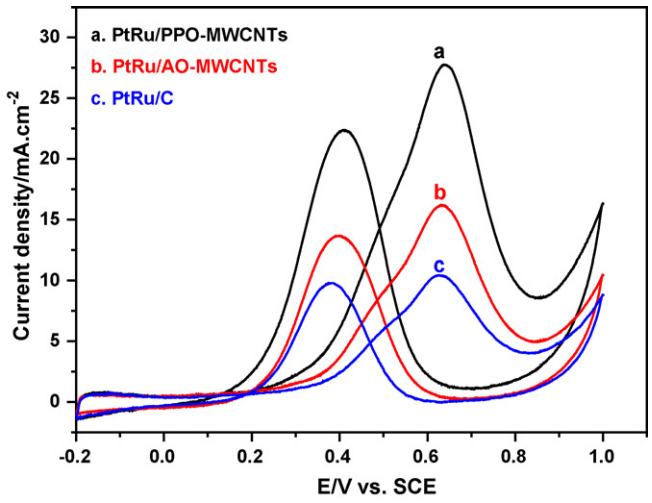

Fig. 8. Cyclic voltammograms of the PtRu/PPO-MWCNTs (a), PtRu/AO-MWCNTs (b), and PtRu/C catalysts (c) in 0.5 M H_2SO_4 + 1.0 M CH_3OH solution saturated by N_2 with scan rate of 50 mV s^{-1}.

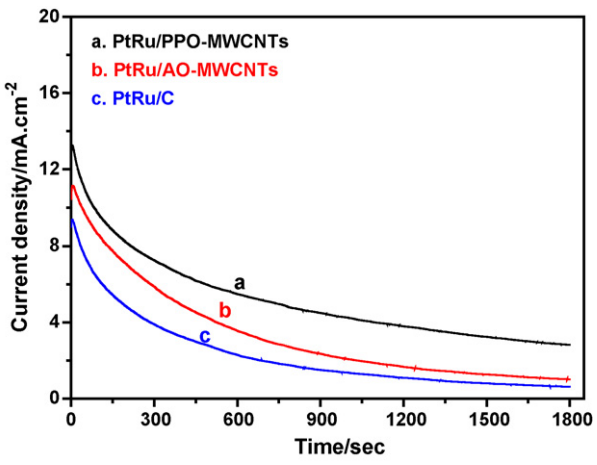

Fig. 9. Chronoamperometry curves of the PtRu/PPO-MWCNTs (a), PtRu/AO-MWCNTs (b), and PtRu/C (c) catalysts in 0.5 M H_2SO_4 + 1.0 M CH_3OH solution saturated by N_2 at room temperature.

3.5. Evaluation of methanol electro-oxidation

Fig. 8 displays the cyclic voltammograms recorded for the oxidation of methanol at a scan rate of 50 mV s^{-1} for PtRu/PPO-MWCNTs, PtRu/AO-MWCNTs, and PtRu/C catalysts. As can be seen from Fig. 8, the voltammograms are similar to those reported in the literature [55,56], and an enhancement in the activity was observed for the PtRu catalyst supported on PPO-MWCNTs evidenced by the lower onset potential and significantly higher oxidation current (seen in Table 1) in the forward sweep. The oxidation peak observed in the reverse scan at around 0.4 V is associated with the oxidation of adsorbed intermediate species in the forward scan. The onset potential for methanol oxidation of PtRu/PPO-MWCNTs is 0.19 V, which shows a negative shift compared to that of PtRu/AO-MWCNTs (0.26 V) and PtRu/C (0.33 V). In principle, with respect to the methanol electro-oxidation mechanism, the onset potential is related to the breaking of C–H bonds and the subsequent removal of the CO_{ads} like intermediates by oxidation with OH_{ads} species supplied by Ru–OH sites [57]. It means that methanol is easy to be oxidized on the PtRu alloy surface of PPO-functionalized MWCNTs. The peak potentials of methanol oxidation are similar, at about 0.64 V, which are close to that reported in the literature [49,58]. In addition, in the static test of the methanol oxidation, the forward peak current density of the PtRu/PPO-MWCNTs (27.8 mA cm^{-2}) is 71.6% higher than that of the PtRu/AO-MWCNTs (16.2 mA cm^{-2}) and 164.8% higher than the PtRu/C (10.5 mA cm^{-2}). The significantly higher anodic current for the reaction on PtRu/PPO-MWCNTs and PtRu/AO-MWCNTs indicates a much higher electrocatalytic activity of MWCNT-supported PtRu electrocatalysts than the carbon supported PtRu electrocatalysts, consistent with that reported in ever before [4,43]. The higher electrocatalytic activity for the methanol oxidation on PtRu/PPO-MWCNTs than PtRu/AO-MWCNTs which most likely due to the higher EAS and improving effect of polypyrrole oligomers in PPO-functionalized MWCNTs for methanol electro-oxidation.

In addition, it is well-known that the ratio of the forward anodic peak current (I_f) to the backward anodic peak current (I_b), I_f/I_b, is an index of the catalyst tolerance to incompletely oxidized species accumulated on the surface of the electrode. A higher ratio indicates more effective removal of the poisoning species on the catalyst surface [58,59]. The I_f/I_b ratio of the PtRu/PPO-MWCNTs was about 1.24, which is higher than that of the PtRu/AO-MWCNTs (1.18) and PtRu/C (1.06) catalysts, showing better catalyst tolerance of the PtRu/PPO-MWCNTs.

Further, to compare the long-term performance of the three catalysts in terms of methanol oxidation, we also conducted using chronoamperometry tests in a solution of 0.5 M H_2SO_4 + 1.0 M CH_3OH for 1800 s. Before the experiment was performed each time, the electrolyte was deaerated with N_2 for 15 min. The superiority of the PtRu/PPO-MWCNTs is further confirmed by the chronoamperometry data (Fig. 9) recorded at a constant potential of 0.55 V at room temperature. The oxidation current decreased continuously for all the catalysts, likely due to the formation of intermediate and poisoning species, such as CO_{ads}, CH_3OH_{ads}, $COOH_{ads}$, and CHO_{ads}, during the methanol oxidation reaction [57,60]. After long-time operation, although the current gradually decayed for all the catalysts, PtRu/PPO-MWCNTs maintained a higher current, and the final current density was 2.81 mA cm^{-2} in comparison to 1.01, and 0.61 mA cm^{-2} obtained for PtRu/AO-MWCNTs, and PtRu/C, respectively. All the above experimental results suggest that higher activity for methanol oxidation can be obtained with the polypyrrole oligomers-functionalized MWCNTs compared to the conventional acid-treated MWCNTs and carbon black.

4. Conclusions

A facile and novel approach to synthesize PtRu/PPO-MWCNTs composite by noncovalent MWCNTs surface with polypyrrole oligomers was reported here. The work represents a new synthesis method of PtRu/MWCNTs electrocatalysts. The synthesis process is simple and without the use of expensive chemicals. Such treatment could preserve the integrity and the electronic structure of MWCNTs. The cyclic voltammetry and chronoamperometry was used to study the properties of the PtRu/PPO-MWCNTs catalyst at room temperature. The higher electrochemical surface area, much better activity, and enhanced stability mostly due to the smaller, well-dispersed PtRu alloy nanoparticles and improving effect of polypyrrole oligomers in PPO-functionalized MWCNTs. It is believe that the enhanced activity of the PtRu/PPO-MWCNTs is surely throwing some light on the research and development of effective DMFC catalysts.

Acknowledgements

This work has been supported by the Natural Science Foundation of Guangxi Province (0728043), Guangxi Ministry of Education

and Innovation Plan in Graduate Education of Guangxi Province (2009106020703M49) for financial support.

References

[1] P. Avouris, M. Freitag, V. Perebeinos, Nat. Photonics 2 (2008) 341–350.
[2] W.A. deHeer, W.S. Bacsa, A. Châtelain, T. Gerfin, R. Humphrey-Baker, L. Forro, D. Ugarte, Science 268 (1995) 845–847.
[3] Z. Zhao, X. Fang, Y. Li, Y. Wang, P.K. Shen, F. Xie, X. Zhang, Electrochem. Commun. 11 (2009) 290–293.
[4] J. Prabhuram, T.S. Zhao, Z.K. Tang, R. Chen, Z.X. Liang, J. Phys. Chem. B 110 (2006) 5245–5252.
[5] L. Li, Y. Xing, J. Phys. Chem. C 111 (2007) 2803–2808.
[6] Y. Xing, L. Li, C.C. Chusuei, R.V. Hull, Langmuir 21 (2005) 4185–4190.
[7] J. Wang, G. Yin, Y. Shao, Z. Wang, Y. Gao, J. Phys. Chem. C 112 (2008) 5784–5789.
[8] X. Li, Y. Liu, L. Fu, L. Cao, D. Wei, Y. Wang, Adv. Funct. Mater. 16 (2006) 2431–2437.
[9] Y. Yan, M. Zhang, K. Gong, L. Su, Z. Guo, L. Mao, Chem. Mater. 17 (2005) 3457–3463.
[10] R.J. Chen, Y. Zhang, D. Wang, H. Dai, J. Am. Chem. Soc. 123 (2001) 3838–3839.
[11] M. Zhang, Y. Yan, K. Gong, L. Mao, Z. Guo, Y. Chen, Langmuir 20 (2004) 8781–8785.
[12] S. Park, S.W. Yoon, H. Choi, J.S. Lee, W.K. Cho, J. Kim, H.J. Park, W.S. Yun, C.H. Choi, Y. Do, I.S. Choi, Chem. Mater. 20 (2008) 4588–4594.
[13] Y. Ma, S.R. Ali, L. Wang, P.L. Chiu, R. Mendelsohn, H. He, J. Am. Chem. Soc. 128 (2006) 12064–12065.
[14] G. Guo, F. Qin, D. Yang, C. Wang, H. Xu, S. Yang, Chem. Mater. 20 (2008) 2291–2297.
[15] M. Liu, T. Zhu, Z. Li, Z. Liu, J. Phys. Chem. C 113 (2009) 9670–9675.
[16] S.-W. Woo, K. Dokko, K. Kanamura, J. Power Sources 185 (2008) 1589–1593.
[17] S.A. Waghuley, S.M. Yenorkar, S.S. Yawale, S.P. Yawale, Sens. Actuators B 128 (2008) 366–373.
[18] A.L. Mohana Reddy, N. Rajalakshmi, S. Ramaprabhu, Carbon 46 (2008) 2–11.
[19] H. Zhao, J. Yang, L. Li, H. Li, J. Wang, Y. Zhang, Int. J. Hydrogen Energy 34 (2009) 3908–3914.
[20] J. Wang, Y. Xu, X. Chen, X. Sun, Compos. Sci. Technol. 67 (2007) 2981–2985.
[21] V. Selvaraj, M. Alagar, Electrochem. Commun. 9 (2007) 1145–1153.
[22] K. Lee, L. Zhang, H. Lui, R. Hui, Z. Shi, J. Zhang, Electrochim. Acta 54 (2009) 4704–4711.
[23] J. Wen, L. Zhou, L. Jin, X. Cao, B.-C. Ye, J. Chromatogr. B 877 (2009) 1793–1798.
[24] J. Dong, Y. Hu, J. Xu, X. Qu, C. Zhao, Electroanalysis 21 (2009) 1792–1798.
[25] X. Lin, Y. Xu, Electrochim. Acta 53 (2008) 4990–4997.
[26] D.E. Raymond, D.J. Harrison, J. Electroanal. Chem. 355 (1993) 115–131.
[27] M.C.D. Jesus, Y. Fu, R.A. Weiss, Polym. Eng. Sci. 37 (1997) 1936–1943.
[28] Y. Jalit, M.C. Rodríguez, M.D. Rubianes, S. Bollo, G.A. Rivas, Electroanalysis 20 (2008) 1623–1631.
[29] J. Zhang, M.Z. Wu, T.S. Pu, Z.Y. Zhang, R.P. Jin, Z.S. Tong, D.Z. Zhu, D.X. Cao, F.Y. Zhu, J.Q. Cao, Thin Solid Films 307 (1997) 14–20.
[30] X. Zhang, J. Zhang, W. Song, Z. Liu, J. Phys. Chem. B 110 (2005) 1158–1165.
[31] S.F. Durrant, N. Marçal, S.G. Castro, R.C.G. Vinhas, M.A.B. De Moraes, J.H. Nicola, Thin Solid Films 259 (1995) 139–145.
[32] Y. Wang, G.A. Sotzing, R.A. Weiss, Chem. Mater. 20 (2008) 2574–2582.
[33] P. Xu, X. Han, C. Wang, D. Zhou, Z. Lv, A. Wen, X. Wang, B. Zhang, J. Phys. Chem. B 112 (2008) 10443–10448.
[34] N.V. Blinova, J. Stejskal, M. Trchová, J. Prokeš, M. Omastová, Eur. Polym. J. 43 (2007) 2331–2341.
[35] T. Jeevananda, Siddaramaiah, N.H. Kim, S.-B. Heo, J.H. Lee, Polym. Adv. Technol. 19 (2008) 1754–1762.
[36] S.-F. Zheng, J.-S. Hu, L.-S. Zhong, L.-J. Wan, W.-G. Song, J. Phys. Chem. C 111 (2007) 11174–11179.
[37] L. Groenendaal, H.W.I. Peerlings, J.L.J. van Dongen, E.E. Havinga, J.A.J.M. Vekemans, E.W. Meijer, Macromolecules 28 (2002) 116–123.
[38] A. Jorio, A.G. Souza Filho, V.W. Brar, A.K. Swan, M.S. Ünlü, B.B. Goldberg, A. Righi, J.H. Hafner, C.M. Lieber, R. Saito, G. Dresselhaus, M.S. Dresselhaus, Phys. Rev. B: Condens. Matter 65 (2002) 121402.
[39] Y. Lin, B. Zhou, K.A. Shiral Fernando, P. Liu, L.F. Allard, Y.-P. Sun, Macromolecules 36 (2003) 7199–7204.
[40] N. Yao, V. Lordi, S.X.C. Ma, E. Dujardin, A. Krishnan, M.M.J. Treacy, T.W. Ebbesen, J. Mater. Res. 13 (1998) 2432–2437.
[41] H. Xu, X. Wang, Y. Zhang, S. Liu, Chem. Mater. 18 (2006) 2929–2934.
[42] H.M. Heise, R. Kuckuk, A.K. Ojha, A. Srivastava, V. Srivastava, B.P. Asthana, J. Raman Spectrosc. 40 (2009) 344–353.
[43] Y. Zhao, X. Yang, J. Tian, Electrochim. Acta 54 (2009) 7114–7120.
[44] S. Wang, X. Wang, S.P. Jiang, Langmuir 24 (2008) 10505–10512.
[45] J. Li, Y. Liang, Q. Liao, X. Zhu, X. Tian, Electrochim. Acta 54 (2009) 1277–1285.
[46] D. Baskaran, J.W. Mays, M.S. Bratcher, Angew. Chem. Int. Ed. 43 (2004) 2138–2142.
[47] M. Dehonor, K. Masenelli-Varlot, A. Gonzalez-Montiel, C. Gauthier, J.Y. Cavaille, H. Terrones, M. Terrones, Chem. Commun. (2005) 5349–5351.
[48] J.T. Moore, J.D. Corn, D. Chu, R. Jiang, D.L. Boxall, E.A. Kenik, C.M. Lukehart, Chem. Mater. 15 (2003) 3320–3325.
[49] Z. Cui, C. Liu, J. Liao, W. Xing, Electrochim. Acta 53 (2008) 7807–7811.
[50] L.-H. Li, W.-D. Zhang, J.-S. Ye, Electroanalysis 20 (2008) 2212–2216.
[51] J.W. Guo, T.S. Zhao, J. Prabhuram, C.W.W.R. Chen, Electrochim. Acta 51 (2005) 754–763.
[52] Y.L. Hsin, K.C. Hwang, C.-T. Yeh, J. Am. Chem. Soc. 129 (2007) 9999–10010.
[53] L. Ren, Y. Xing, Electrochim. Acta 53 (2008) 5563–5568.
[54] Z.-B. Wang, G.-P. Yin, J. Zhang, Y.-C. Sun, P.-F. Shi, J. Power Sources 160 (2006) 37–43.
[55] R. Chetty, W. Xia, S. Kundu, M. Bron, T. Reinecke, W. Schuhmann, M. Muhler, Langmuir 25 (2009) 3853–3860.
[56] H. Zhao, L. Li, J. Yang, Y. Zhang, J. Power Sources 184 (2008) 375–380.
[57] R. Chetty, S. Kundu, W. Xia, M. Bron, W. Schuhmann, V. Chirila, W. Brandl, T. Reinecke, M. Muhler, Electrochim. Acta 54 (2009) 4208–4215.
[58] L. Wang, S. Guo, J. Zhai, S. Dong, J. Phys. Chem. C 112 (2008) 13372–13377.
[59] Q. Shen, L. Jiang, H. Zhang, Q. Min, W. Hou, J.-J. Zhu, J. Phys. Chem. C 112 (2008) 16385–16392.
[60] Y.-J. Gu, W.-T. Wong, Langmuir 22 (2006) 11447–11452.